Supplemental Data

Table S1, Related to Figures 1 and 2. Data collection and refinement statistics (molecular replacement)

	Trimer (PDB 4WOL)	Tetramer (PDB 4WO1)
Data collection		
Space group	P 2_1 2_1 2_1	P 2_1 2_1 2
Cell dimensions		
a, *b*, *c* (Å)	20.78 35.71 101.07	50.80 43.69 50.61
α, β, γ (°)	90 90 90	90 90 90
Resolution (Å)	33.67 - 1.77 (1.83 - 1.77)*	33.12 - 2.14 (2.22 - 2.14)*
R_{merge}	0.1357 (0.9853)	0.1374 (0.9379)
$CC_{1/2}$ #	0.997 (0.856)	0.997 (0.909)
$I / \sigma I$	22.26 (2.40)	15.46 (2.62)
Completeness (%)	95.48 (100.00)	95.74 (83.15)
Redundancy	13.0 (13.4)	6.6 (7.0)
Refinement		
Resolution (Å)	33.67 - 1.77 (1.83 - 1.77)	33.12 - 2.14 (2.22 - 2.14)
No. unique reflections	7502 (741)	6316 (648)
R_{work} / R_{free}	0.1812 (0.2326) / 0.2222 (0.2701)	0.2329 (0.2459) / 0.2988 (0.3668)
No. atoms		
Protein	660	880
Ligand/ion	101	124
Water	37	31
B-factors		
Protein	26.50	30.60
Ligand/ion	47.40	58.00
Water	44.30	47.00
R.m.s. deviations		
Bond lengths (Å)	0.008	0.007
Bond angles (°)	0.90	0.94

*Values in parentheses are for highest-resolution shell. Each structure was solved from a single crystal. #Pearson correlation coefficient between equivalent reflection sets in two randomly selected halves of the unmerged experimental data (Karplus and Diederichs, 2012).

Table S2, Related to Figure 3 and S3: Interfaces in trimer lattice

Chain 1	# atoms in interface	Chain 2	# atoms in interface	Symmetry op	Buried area, Å2	ΔiG kcal/mol	CSS*
C	42	B	40	x,y,z	422	-10.7	0.148
C	45	A	45	x,y,z	418	-9.2	0.148
Potassium	1	A	11	x,y,z	67	-38.6	0.756
Potassium	1	C	10	x,y,z	63	-36.3	0.756
Potassium	1	B	11	x,y,z	61	-33.2	0.756
B	32	A	36	x,y,z	329	-9.3	0.096
B	49	A	44	x-1,y,z	421	-12.2	1.000
C	19	A	21	x-1,y,z	193	-5.6	0.000
B	9	C	12	x-1,y,z	105	-2.3	0.000
B	36	A	32	x-1/2,-y+1/2,-z+1	343	-10.3	1.000
B	21	B	15	x-1/2,-y+1/2,-z+1	187	-5.0	0.000
A	7	A	7	x-1/2,-y+1/2,-z+1	74	-2.2	0.000
C	25	C	17	x-1/2,-y+3/2,-z+1	238	-6.8	0.000
C	10	A	15	x-1/2,-y+3/2,-z+1	143	-4.5	0.000
C	10	A	8	-x+3/2,-y+1,z-1/2	75	0.7	0.000
A	6	A	6	-x+3/2,-y+1,z-1/2	65	1.2	0.000
A	1	B	1	-x+3/2,-y+1,z-1/2	2	0.0	0.000
B	4	A	4	-x+1/2,-y+1,z-1/2	36	0.3	0.000
B	4	B	1	-x+1/2,-y+1,z-1/2	25	-0.9	0.000

*Complex significance score: 1 indicates a high relative significance for the analyzed assembly; 0 indicates low relative significance. Highlighted value criteria: Buried surface area > 10% of total surface area of smallest partner, ΔiG < -10 kcal/mol, CSS > 0. Table modified from PDBePISA-generated output (Krissinel and Henrick, 2007).

Table S3, Related to Figure 3 and S3: Interfaces in tetramer lattice

Chain 1	# atoms in interface	Chain 2	# atoms in interface	Symmetry op	Buried area, Å2	ΔiG kcal/mol	CSS*
C	57	B	47	x,y,z	569	-12.2	1.000
D	58	A	46	x,y,z	559	-11.7	1.000
D	27	B	30	x,y,z	273	-7.0	0.497
C	27	A	28	x,y,z	258	-6.6	0.497
B	25	A	26	x,y,z	266	-4.6	0.365
Calcium	1	B	6	x,y,z	31	-4.8	0.323
Calcium	1	A	4	x,y,z	29	-4.7	0.311
Calcium	1	D	5	x,y,z	19	-2.7	0.181
C	41	D	41	-x-1/2,y-1/2,-z-1	463	-12.6	1.000
A	19	B	14	-x-1/2,y-1/2,-z-1	172	-5.4	0.113
A	11	D	16	-x-1/2,y-1/2,-z-1	155	-4.2	0.164
C	15	B	10	-x-1/2,y-1/2,-z-1	129	-3.7	0.164
A	3	A	4	-x-1/2,y-1/2,-z-1	32	-1.0	0.000
B	4	B	3	-x-1/2,y-1/2,-z-1	27	-0.7	0.000
C	13	D	12	x-1/2,-y+1/2,-z-1	167	-5.4	0.277
B	10	D	7	x-1/2,-y+1/2,-z-1	99	-3.1	0.056
D	7	D	2	x,y,z-1	34	-0.4	0.000
C	9	C	5	x,y,z-1	60	0.0	0.000
B	1	A	1	x,y,z-1	1	0.0	0.000
A	1	B	1	x,y,z-1	16	0.4	0.000
C	7	C	7	-x-1,-y,z	87	-2.8	0.072

*Complex significance score: 1 indicates a high relative significance for the analyzed assembly; 0 indicates low relative significance. Highlighted value criteria: Buried surface area > 10% of total surface area of smallest partner, ΔiG < -10 kcal/mol, CSS > 0. Table modified from PDBePISA-generated output (Krissinel and Henrick, 2007).

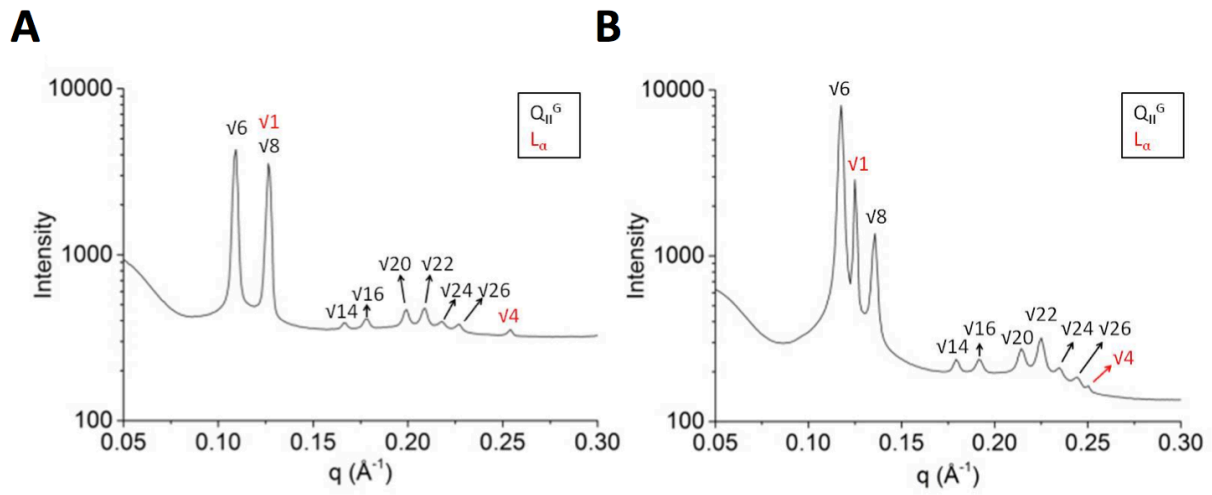

Figure S1, Related to Figures 1 and 2. Small-angle X-ray diffraction analysis of lipidic cubic phase formation. The 1D small-angle X-ray diffraction (intensity on a logarithmic scale against q) is shown for the two conditions that produced the crystals used to solve DAP12-TM structures. **(A)** Image taken 6 days after setup using monoolein with 10% cholesterol, 40 mg/ml DAP12-TM, 12.4 % (w/v) PEG 3350 and 0.149 M potassium thiocyanate in excess water. For the gyroid cubic Q_{II}^{G} phase with lattice parameter 141.5 Å the $6^{1/2}$, $8^{1/2}$, $14^{1/2}$, $16^{1/2}$, $20^{1/2}$, $22^{1/2}$, $24^{1/2}$ and $26^{1/2}$ reflections are visible. For the fluid lamellar L_{α} phase with lattice parameter 49.2 Å the $1^{1/2}$ and $4^{1/2}$ reflections are visible. The $8^{1/2}$ reflection of Q_{II}^{G} and $1^{1/2}$ reflection of L_{α} are superposed. **(B)** Image taken 1 day after setup using monoolein, 70 mg/ml DAP12-TM, 0.1 M bis-tris propane chloride (pH 6.07), 19.7 % (w/v) PEG 3350 and 0.269 M calcium chloride in excess water. For the Q_{II}^{G} phase with lattice parameter 131.5 Å the $6^{1/2}$, $8^{1/2}$, $14^{1/2}$, $16^{1/2}$, $20^{1/2}$, $22^{1/2}$, $24^{1/2}$ and $26^{1/2}$ reflections are visible. For the L_{α} phase with lattice parameter 50.1 Å the $1^{1/2}$ and $4^{1/2}$ reflections are visible.

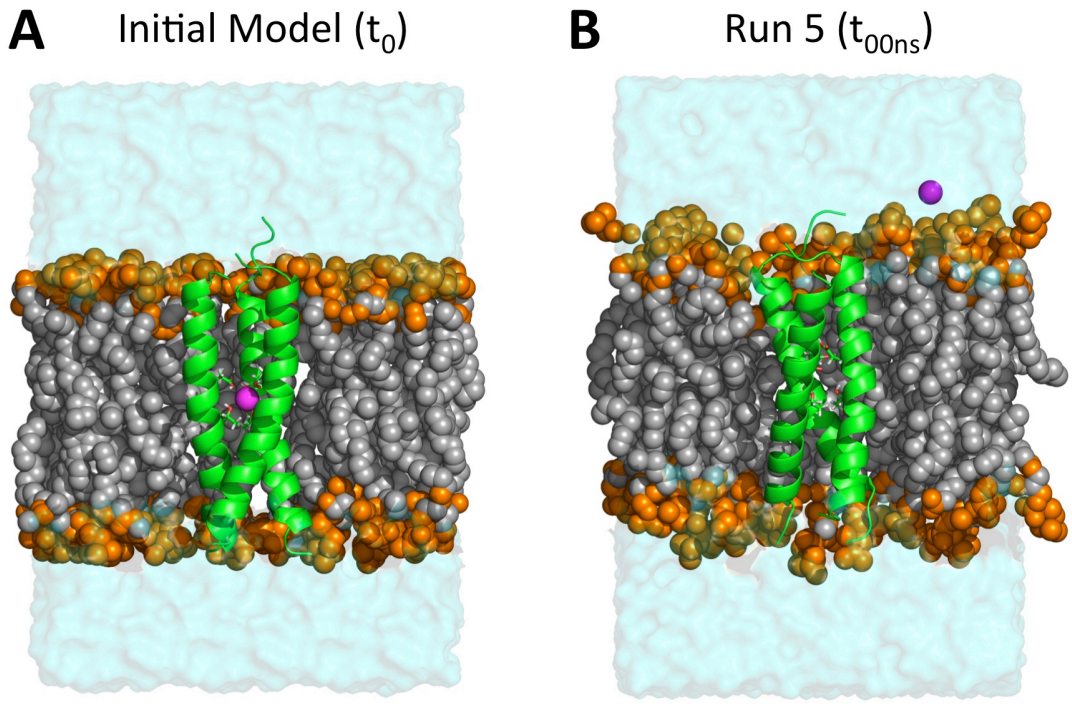

Figure S2, Related to Figure 1. Loss of K^+ ion coordination from DAP12-TM trimer simulations with no ionized aspartic acids. Snapshots from simulations shown in Figure 1A (0 Asp^-). **(A)** The initial model (green ribbons) with bound K^+ ion (magenta) is shown in the model POPC bilayer (orange headgroups, gray tails) surrounded by bulk water (cyan). **(B)** Coordinated K^+ was lost to the bulk solvent by the end of the 200 ns simulation in three of the five independent trajectories. One representative structure is shown.

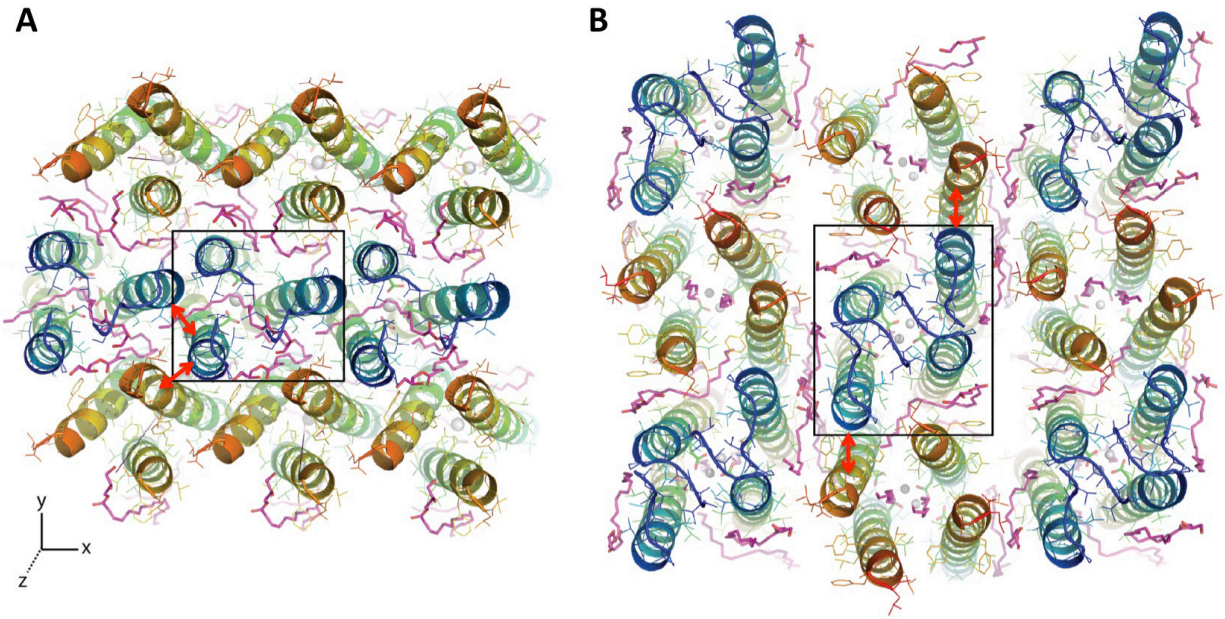

Figure S3, Related to Figure 3. Arrangement of DAP12-TM trimers and tetramers within a single layer. Views of trimeric **(A)** and tetrameric **(B)** DAP12-TM complexes are shown looking down an axis that is normal to the membrane plane. Helices are colored in a spectrum of blue (amino-terminal) to red (carboxy-terminal) to show directionality in the packing. Monoolein is shown in magenta stick representation. Coordinated cations are shown in grey spheres. One asymmetric unit is boxed in each image. Major contacts to DAP12 chains in neighboring asymmetric units are indicated by red arrows.

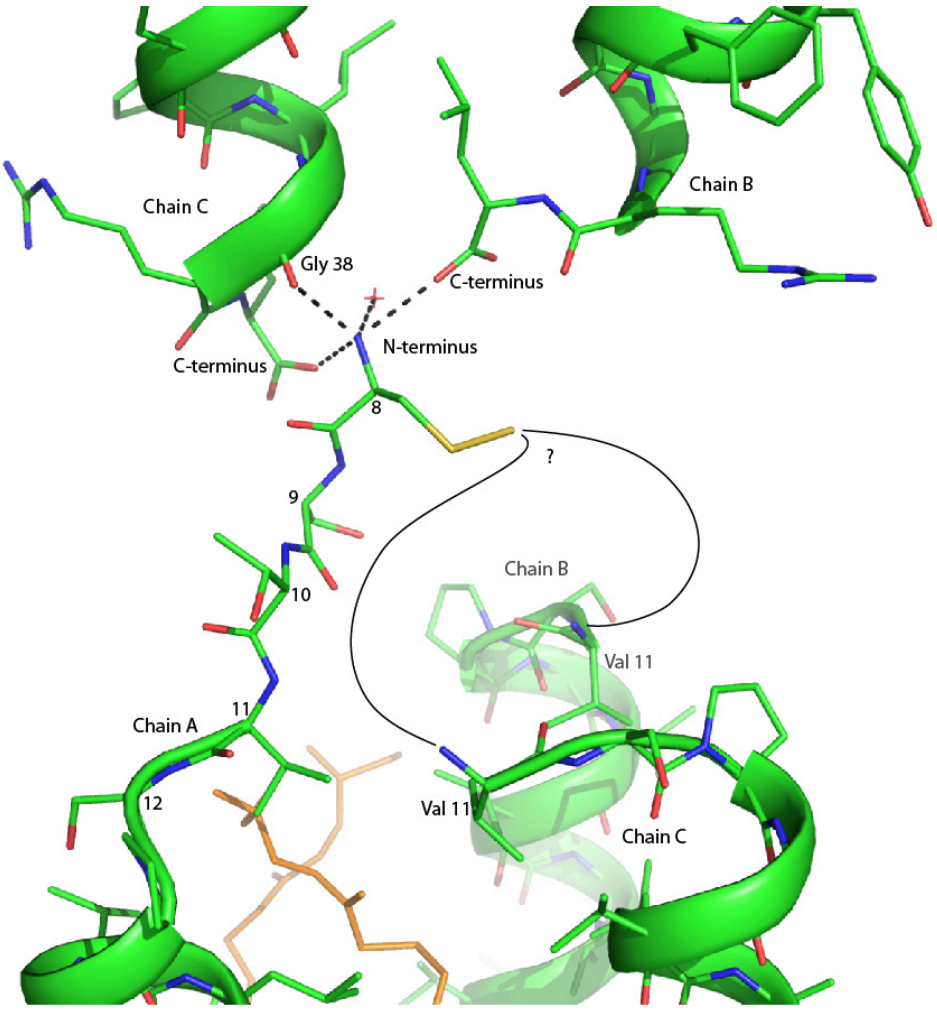

Figure S4, Related to Figure 3. Contacts between lamellar layers in trimeric DAP12 crystals. The chain A N-terminus extends up towards Chain C and Chain B in the layer above. Residues 8 through 12 of Chain A are numbered accordingly. The N-terminal free amine makes contact with Chain C Gly38 and the C-terminal oxygens of Chain C and Chain B. The disufide bond is shown in yellow, however density could not be traced to show connectivity to Chain B or Chain C in the asymmetric unit. Structured monoolein is shown in orange, and a structured water also coordinated by the Chain A N-terminal amine is depicted as a red cross.

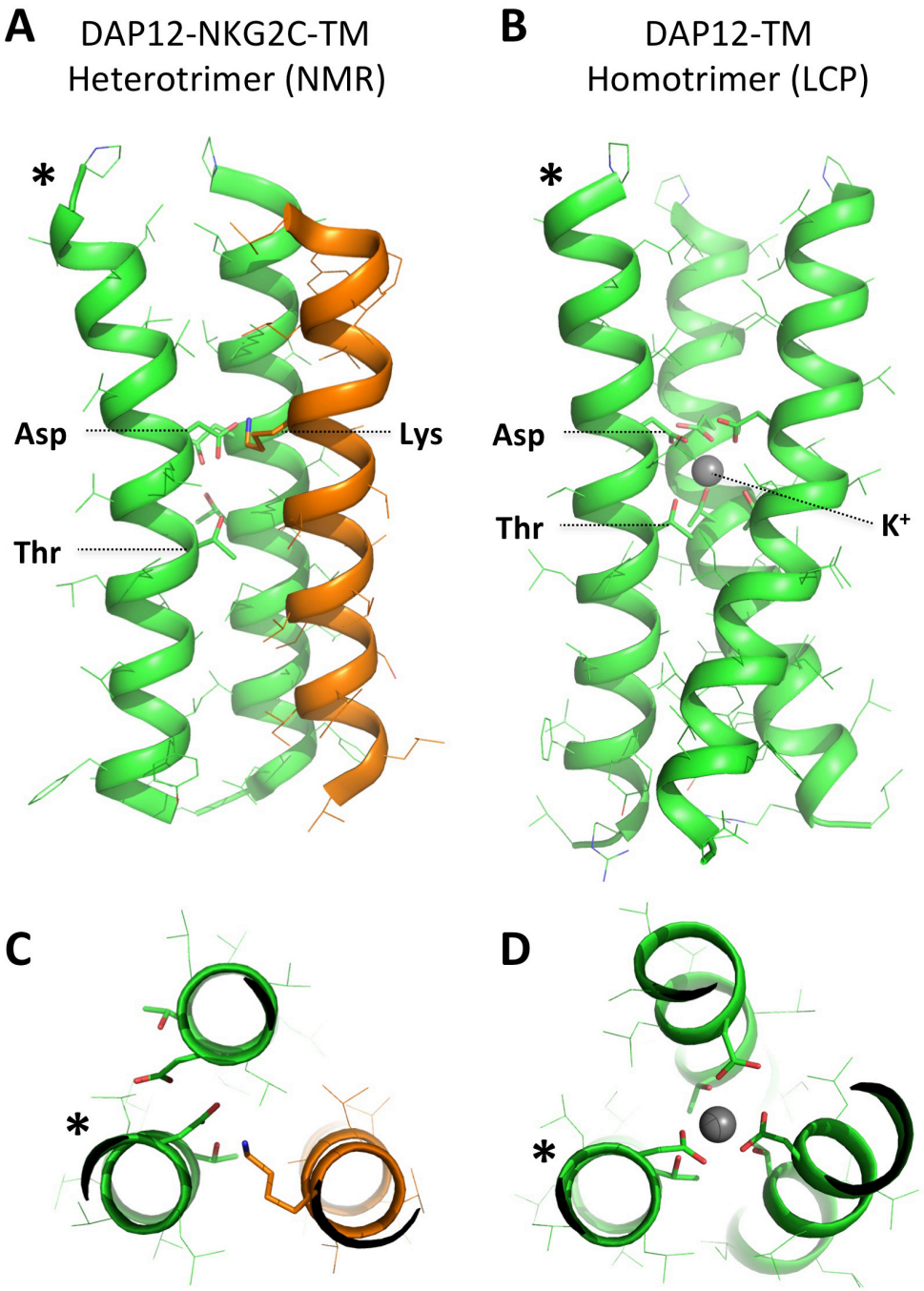

Figure S5, Related to Figure 5. Comparison of trimeric arrangements in solution NMR and LCP crystal structures. Side (**A** and **B**) and top (**C** and **D**) views are shown for the DAP12-NKG2C-TM solution NMR structure (**A** and **C**; PDB 2L35, model 7) and the DAP12-TM homotrimer crystal structure (**B** and **D**; PDB 4WOL). NKG2C-TM in the NMR structure is shown in orange ribbon and all DAP12-TMs are shown in green ribbon. NMR and crystal structures are approximately aligned on the DAP12 chain marked (*).

Supplemental Experimental Procedures

Lipidic cubic phase preparation and crystallization of DAP12

DAP12-TM dimer peptide was weighed and mixed with the appropriate volume of monoolein (Nu-Chek Prep) with or without 10% (w/v) cholesterol (Sigma-Aldrich). 500 µl of hexafluoroisopropanol (HFIP; Sigma-Aldrich) was added with brief vortexing until a homogeneous solution was reached. Solvent was removed under streaming nitrogen and the sample was dried under vacuum overnight. The peptide/lipid mixture was gently heated (50°C) until liquid and mixed 3:2 with ultrapure water using coupled 100 µl gastight Hamilton syringes (Formulatrix) until a homogeneous phase was achieved. Final DAP12-TM concentration was 70 mg/ml in initial screens and subsequently tested at lower concentrations. The LCP mixture was dispensed at room temperature in 200 nl drops onto 96-well glass plates (Molecular Dimensions) with 1000 µl of precipitant solution using a mosquito LCP (TTP Labtech) robot. Plates were sealed and kept at 20°C in a Gallery 700 incubator coupled to a Minstrel HTUV imaging system (Rigaku) for monitoring of crystal formation.

Small angle X-ray scattering (SAXS) analysis

The lipid mesophase structure was determined *in situ* within a 96-well Laminex UV plastic plate sealed with a Laminex UV plastic cover (Molecular Dimensions). The plate was contained within a temperature-controlled custom-designed plate holder and mounted directly onto the SAXS/WAXS beamline at the Australian Synchrotron for structural analysis. Data for Figure S1A was obtained using a beam of wavelength 1.240 Å (10.0 keV), beam dimensions of 300 x 200 µm, and a typical flux of 1.2 x 10^{13} photons/s. 2D diffraction images were recorded at 20°C on a Pilatus 1M detector; the exposure time was 0.5s. Data for Figure S1B were obtained using a beam of wavelength 1.127 Å (11.0 keV), and an exposure time of 1.0s. Many orders of diffraction were observed allowing unambiguous identification of the cubic phases. A custom-designed IDL-based software package (AXcess) was used for analysis of the X-ray images produced. A more extensive description of SAXS analysis methods can be found in (van 't Hag et al., 2014).

Data collection and structure determination

Crystals were harvested directly from the crystallization plate and frozen in liquid nitrogen without the addition of a cryoprotecting solution. Data were collected at the Australian Synchrotron on the MX2 beamline at a wavelength of 0.9537 Å and temperature of 100 K. The data were indexed and scaled using HKL2000 (Otwinowski and Minor, 1997). Structure factor amplitudes were obtained using Truncate (French and Wilson, 1978) (CCP4 Program Suite (Winn et al., 2011)). The DAP12 trimer structure was solved with Phaser (McCoy et al., 2007) by molecular replacement using Glycophorin A (MacKenzie et al., 1997) (PDB1AFO, chain A, state 1) as the search model. Iterative rounds of refinement were performed in PHENIX (Adams et al., 2010) (XYZ coordinates, individual B factors, simulated annealing and TLS parameters) and model building in Coot (Emsley et al., 2010). Chain A from the DAP12 trimer structure was used to solve the tetramer structure by molecular replacement using Phaser. PHENIX and Coot were also used to refine and build the tetramer structure. In the early stages of refinement, non-crystallographic symmetry was defined assuming all four chains in the asymmetric unit were equivalent. After several rounds of refinement it was observed that the side-chain conformation of Phe36 was not equivalent in all four chains, indicating that NCS would be better defined

assuming two equivalent dimers. In the final stages of refinement NCS restraints were eliminated with negligible effects on the R-free value. Ramachandran analysis of the trimer structure revealed 100% of residues in favored regions, while in the tetrameric structure 99.15% of residues were in favored regions and 0.85% in allowed regions. No residues in either structure were outliers.

Molecular dynamics simulations

Molecular dynamics simulations were performed on DAP12 trimer and tetramer structures in different ionization states of the aspartic acid residue 23: the trimer with coordinated potassium ion in four different ionization states (0, 1, 2, or 3 deprotonated aspartic acids) and the tetramers with one or two coordinated calcium ions in two ionization states (two deprotonated and two protonated aspartic acids or four deprotonated aspartic acids). These models were used to build the initial systems in a POPC bilayer by following the general procedure of bilayer system building and equilibration in *Membrane Builder* (Jo et al., 2007; Jo et al., 2009) at the CHARMM-GUI website (http://www.charmm-gui.org/input/membrane) (Jo et al., 2008). The initial systems were composed of each DAP12 model with coordinated ions, 48 POPC lipids in each leaflet, the bulk water, and the ions in the bulk aqueous phase (150 mM KCl and 50 mM $CaCl_2$ for trimers and tetramers, respectively). Each system was equilibrated using CHARMM (Brooks et al., 2009) by following *Membrane Builder*'s standard six-step protocol (Jo et al., 2007), where the restraints on the components were gradually decreased during the simulations. We repeated the procedure with a different initial seed number to prepare five independent replicas for each model of DAP12 trimer and tetramer. After equilibration, a 200-ns NAMD (Phillips et al., 2005) production run was performed for each system without any restraints under the constant temperature and pressure condition (NPT) at 303.15 K and 1 bar, respectively. The temperature was maintained by using Langevin dynamics with a Langevin coupling coefficient set to 1 ps^{-1} and the pressure was controlled by a Nosé-Hoover Langevin-piston (Feller et al., 1995; Martyna et al., 1994) with a piston period of 50 fs and a piston decay of 25 fs. We used an integration time step of 2 fs with SHAKE algorithm (Ryckaert et al., 1977). The van der Waals interactions were smoothly switched off over 10-12 Å by a force-switching function (Steinbach and Brooks, 1994). The particle-mesh Ewald method (Essmann et al., 1995) was used for the calculation of the long-range electrostatic interactions, where a mesh size of around 1 Å was used for fast Fourier transformation and sixth order B-spline interpolation.

Cellular DAP12 analysis

Human DAP12 with a C-terminal haemagglutinin (HA) epitope tag (YDYDVPDYA) was cloned into the pCI-neo expression vector (Promega). Defined amounts of pCI-neo-DAP12-HA (18, 6 and 2 ng/well in Figure 4A) were mixed with carrier DNA to 5.1 μg/9.5cm^2 and complexed with calcium phosphate for introduction into 293T cells at 50% confluence in 6-well culture plates. Cells were lysed two days post-transfection with 1% Triton X-100, 0.5% sodium deoxycholate, 0.1% SDS, 150 mM sodium chloride, 50 mM Tris pH 8.0 (RIPA buffer) containing protease inhibitors (P8340, Sigma-Aldrich) and 50 mM iodoacetamide. DAP12-HA was isolated from the lysate by immunoprecipitation with anti-HA agarose beads (clone HA-7, Sigma-Aldrich), separated by SDS-PAGE and transferred to PVDF for western blot analysis. Blots were probed with anti-HA-bio (3F10, Roche Life Science) followed by streptavidin horseradish peroxidase and bands were visualized using a chemiluminescent substrate (Western Lightning Plus ECL, Perkin Elmer).

In vitro translation

Synthetic mRNAs encoding full-length human DAP12 with a mouse H-2K^b leader sequence (MVPCTLLLLLAAALAPTQTRA) and a C-terminal HA epitope tag and human KIR2DS3 with a mouse H-2K^b leader sequence and 20-amino-acid transmembrane sequence replaced with LLLLLLLLKLLLLLLLLLLL were transcribed from a modified pSP64 vector using the RiboMax T7 Large-Scale RNA Production kit and methyl-^{7}G cap analogue (Promega). Capped and polyadenylated mRNA was purified using the RNeasy kit (Qiagen) according to the manufacturer's instructions. Each 50 µl *in vitro* translation reaction contained 200-600 ng mRNA (empirically determined to match protein levels across all mutants), 35 µl nuclease-treated rabbit reticulocyte lysate (Promega), 1 µl amino acid mixture minus methionine/cysteine (Promega), 1 µl RNase-In RNase inhibitor (Promega), 4 µl of [^{35}S]-labeled methionine/cysteine mixture (Perkin Elmer), and 4 µl ER microsomes isolated from a murine B-cell hybridoma (IVD12) as previously described (Call et al., 2002). An initial translation period of 30 minutes at 30°C was followed by a 1- or 2-hour assembly period at 30°C after addition of oxidized glutathione to 4 mM final concentration. Detergent extraction of washed ER microsomes and immunoprecipitation with anti-HA agarose beads was carried out as previously described (Call et al., 2010). Labeled products were separated by SDS-PAGE and transferred to PVDF for phosphor imaging analysis.

Supplemental References

Adams, P.D., Afonine, P.V., Bunkoczi, G., Chen, V.B., Davis, I.W., Echols, N., Headd, J.J., Hung, L.W., Kapral, G.J., Grosse-Kunstleve, R.W.*, et al.* (2010). PHENIX: a comprehensive Python-based system for macromolecular structure solution. Acta Crystallogr D *66*, 213-221.

Brooks, B.R., Brooks, C.L., Mackerell, A.D., Nilsson, L., Petrella, R.J., Roux, B., Won, Y., Archontis, G., Bartels, C., Boresch, S.*, et al.* (2009). CHARMM: The biomolecular simulation program. Journal of Computational Chemistry *30*, 1545-1614.

Call, M.E., Pyrdol, J., Wiedmann, M., and Wucherpfennig, K.W. (2002). The organizing principle in the formation of the T cell receptor-CD3 complex. Cell *111*, 967-979.

Call, M.E., Wucherpfennig, K.W., and Chou, J.J. (2010). The structural basis for intramembrane assembly of an activating immunoreceptor complex. Nature immunology *11*, 1023-1029.

Emsley, P., Lohkamp, B., Scott, W.G., and Cowtan, K. (2010). Features and development of Coot. Acta Crystallogr D *66*, 486-501.

Essmann, U., Perera, L., Berkowitz, M.L., Darden, T., Lee, H., and Pedersen, L.G. (1995). A smooth particle mesh Ewald method. The Journal of Chemical Physics *103*, 8577-8593.

Feller, S.E., Zhang, Y., Pastor, R.W., and Brooks, B.R. (1995). Constant pressure molecular dynamics simulation: The Langevin piston method. The Journal of Chemical Physics *103*, 4613-4621.

French, S., and Wilson, K. (1978). Treatment of Negative Intensity Observations. Acta Crystallogr A *34*, 517-525.

Jo, S., Kim, T., and Im, W. (2007). Automated Builder and Database of Protein/Membrane Complexes for Molecular Dynamics Simulations. PloS one *2*, e880.

Jo, S., Kim, T., Iyer, V.G., and Im, W. (2008). CHARMM-GUI: A web-based graphical user interface for CHARMM. Journal of Computational Chemistry *29*, 1859-1865.

Jo, S., Lim, J.B., Klauda, J.B., and Im, W. (2009). CHARMM-GUI Membrane Builder for Mixed Bilayers and Its Application to Yeast Membranes. Biophysical journal *97*, 50-58.

Karplus, P.A., and Diederichs, K. (2012). Linking crystallographic model and data quality. Science *336*, 1030-1033.

Krissinel, E., and Henrick, K. (2007). Inference of macromolecular assemblies from crystalline state. Journal of molecular biology *372*, 774-797.

MacKenzie, K.R., Prestegard, J.H., and Engelman, D.M. (1997). A transmembrane helix dimer: structure and implications. Science *276*, 131-133.

Martyna, G.J., Tobias, D.J., and Klein, M.L. (1994). Constant pressure molecular dynamics algorithms. The Journal of Chemical Physics *101*, 4177-4189.

McCoy, A.J., Grosse-Kunstleve, R.W., Adams, P.D., Winn, M.D., Storoni, L.C., and Read, R.J. (2007). Phaser crystallographic software. Journal of applied crystallography *40*, 658-674.

Otwinowski, Z., and Minor, W. (1997). Processing of X-ray diffraction data collected in oscillation mode. Methods in Enzymology, Macromolecular Crystallography, Pt A *276*, 307-326.

Phillips, J.C., Braun, R., Wang, W., Gumbart, J., Tajkhorshid, E., Villa, E., Chipot, C., Skeel, R.D., Kalé, L., and Schulten, K. (2005). Scalable molecular dynamics with NAMD. Journal of Computational Chemistry *26*, 1781-1802.

Ryckaert, J.-P., Ciccotti, G., and Berendsen, H.J.C. (1977). Numerical integration of the cartesian equations of motion of a system with constraints: molecular dynamics of n-alkanes. Journal of Computational Physics *23*, 327-341.

Steinbach, P.J., and Brooks, B.R. (1994). New spherical-cutoff methods for long-range forces in macromolecular simulation. Journal of Computational Chemistry *15*, 667-683.

van 't Hag, L., Darmanin, C., Le, T.C., Mudie, S., Conn, C.E., and Drummond, C.J. (2014). In Meso Crystallization: Compatibility of Different Lipid Bicontinuous Cubic Mesophases with the Cubic Crystallization Screen in Aqueous Solution. Crystal growth & design *14*, 1771-1781.

Winn, M.D., Ballard, C.C., Cowtan, K.D., Dodson, E.J., Emsley, P., Evans, P.R., Keegan, R.M., Krissinel, E.B., Leslie, A.G., McCoy, A.*, et al.* (2011). Overview of the CCP4 suite and current developments. Acta crystallographica Section D, Biological crystallography *67*, 235-242.